



**HAL**  
open science

# Solvent-Driven Biomimetic Soft Sensors and Actuators

Quan Sun, Cédric Ayela, Damien Thuau

► **To cite this version:**

Quan Sun, Cédric Ayela, Damien Thuau. Solvent-Driven Biomimetic Soft Sensors and Actuators. Advanced Materials Interfaces, In press, pp.2201349. 10.1002/admi.202201349 . hal-03875919

**HAL Id: hal-03875919**

**<https://hal.science/hal-03875919>**

Submitted on 13 Nov 2023

**HAL** is a multi-disciplinary open access archive for the deposit and dissemination of scientific research documents, whether they are published or not. The documents may come from teaching and research institutions in France or abroad, or from public or private research centers.

L'archive ouverte pluridisciplinaire **HAL**, est destinée au dépôt et à la diffusion de documents scientifiques de niveau recherche, publiés ou non, émanant des établissements d'enseignement et de recherche français ou étrangers, des laboratoires publics ou privés.

# Solvent-Driven Biomimetic Soft Sensors and Actuators

Quan Sun, Cédric Ayela, and Damien Thuau\*

The emergence of soft actuators that exhibit large, complex, programmable, and reversible shape deformation is of fundamental interest having potential applications in optics, medicals, and robotics fields. However, existing soft actuators are generally driven by only few given external stimuli such as temperature, humidity, or light which limit their interactions with their surroundings. Here, biomimetic soft actuators that respond to a variety of solvent vapors via programmable motion studied by Finite Element Modeling (FEM) are presented. A versatile micromachining process is used to fabricate these biomimetic soft actuators able to bend, curve, and twist in different manners according to their designs mimicking stamen, seed pots, and petals of *Bauhinia variegata* and *Dendrobium orchids*. The kinetic parameters of the transient response and recovery actuation are taken as the input feature in principal component analysis (PCA) to discriminate analyte molecules. Finally, to broaden the accessible 3D motions and thus functions of these smart actuators, an origami approach is employed to provide further flexibility and novel controlled structural changes in continuum structures such as snake-like soft actuators, walkers, and grippers.

their environments such as pH,<sup>[6,7]</sup> temperature,<sup>[8–10]</sup> humidity,<sup>[11–15]</sup> and light<sup>[16–18]</sup> by way of compliant motion. They present great potential to fulfill sensing and actuation requirements in the field of artificial muscles, energy generators, valves, grippers, swimmers, and walkers. Recently, solvent vapor-driven soft actuators have been reported<sup>[19–21]</sup> and seen as promising devices for human–environment interaction. Currently, molecule absorption-driven soft actuators are often limited to water, ethanol, and acetone vapors preventing their use in advanced wearable applications. Recent progresses in engineering smart materials<sup>[22–25]</sup> and their applications as soft actuators<sup>[26]</sup> exhibiting complex, 3-dimensional shape deformations have been broadly reviewed for a more comprehensive analysis. In brief, 3-dimensional (3D) deformations can be induced either by applying non-uniform external stimuli onto an isotropic

## 1. Introduction

Nature is an incessant source of inspiration for engineering bioinspired soft sensors and actuators.<sup>[1]</sup> Among natural organisms, plants exhibit a panel of complex shape transformations or movements in response to interactions with their environments, i.e., curving of tendrils or bracts around a wire, blooming of flowers and shaping of leaves at different stages of their growth. Utilizing natural concepts sparks inspiration and innovation for the design of a modern class of soft synthetic systems that can adapt their shape in simple to complex ways mimicking living systems.<sup>[2–5]</sup> Soft synthetic bioinspired systems often referred to soft robots can morph in response to

structure or via the conception of anisotropic actuators, the latter being the favorable option to induce programmable and controllable deformations. To date, a large panel of heterogeneous structures such as bilayer, gradient, and patterned structures have been reported.<sup>[27]</sup> Herein, we leverage this approach through the development of solvent responsive biomimetic soft actuators able to precisely curve and twist in a controlled manner. They are based on rigid oriented microstripes of SU-8 photosensitive epoxy resin patterned by photolithography on one or two sides of polydimethylsiloxane (PDMS) thin films to mimic living organisms. The resulting micro-structured soft actuators are compared to bilayer actuators that consist in an active layer expanding under volatile organic compounds (VOCs) exposure and deposited on top of a passive layer. PDMS, which belongs to the class of silicones, is an excellent candidate material for high-performance solvent responsive soft actuators due to its inherent mechanical flexibility and durability against repeated deformation. PDMS exhibits high thermal and humidity stability in addition to an ability to swell when exposed to VOCs. In fact, PDMS was often used in the field of analytical chemistry<sup>[28]</sup> and reported for instance as an efficient matrix material for sampling analyte molecules in aqueous medium.<sup>[29]</sup> Although the swelling of PDMS is not desired for numbers of applications, it provides excellent opportunities as actuation material in molecular-driven soft devices. Various self-folding microstructures based on polymeric materials among them PDMS have been reported with actuation mechanisms ranging from thermal, magnetic, stress mismatch between bilayers and surface tension driven structures.<sup>[30–35]</sup>

Q. Sun, C. Ayela, D. Thuau  
CNRS

Bordeaux INP  
Laboratoire de l'Intégration du Matériau au Système UMR 5218  
Université de Bordeaux  
16 Avenue Pey Berland, Pessac Cedex 33607, France  
E-mail: damien.thuau@u-bordeaux.fr

 The ORCID identification number(s) for the author(s) of this article can be found under <https://doi.org/10.1002/admi.202201349>.

© 2022 The Authors. Advanced Materials Interfaces published by Wiley-VCH GmbH. This is an open access article under the terms of the Creative Commons Attribution License, which permits use, distribution and reproduction in any medium, provided the original work is properly cited.

DOI: 10.1002/admi.202201349

Concretely, we report a comprehensive study by means of finite element modeling (FEM) that reveals the relationship between optimal material properties and relevant geometries for predictive 3D motion of soft actuators. Based on these FEM results, solvent responsive anisotropic PDMS/SU-8 soft actuators moving in controlled 3D manners are fabricated. Their actuation performance as a function of several VOCs are analyzed from video recordings using a developed motion trackers software. Their transient responses were fitted with an analytical model to extract kinetic features related to their motion. These parameters are used in principal component analysis (PCA) to discriminate various analyte molecules. We also report an origami approach by adding creases that behave as hinges in soft structures providing further flexibility and novel controlled motion in specific directions in soft continuum structures such as snake like actuators, grippers and walkers. We believe that the presented solvent responsive biomimetic soft actuators may inspire the design of future advanced soft actuators and sensors. More precisely, snake like soft actuator could find application in minimally invasive surgery where programmable accurate continuum soft structures are highly required. Soft grippers could be added to rigid arms to improved safety, especially in scenarios that involve human-machine interaction. In the specific case of solvent driven soft actuators, they could be used in harsh gaseous environment to manipulate objects or open and close capillaries. In addition, they could be used as sensors to monitor VOC concentration in an environment or decontaminate them by sorption.

## 2. 3D Actuation Prediction by Finite Element Modeling (FEM)

To validate the principle of solvent responsive biomimetic 3D soft actuators, their mechanical deformations were studied and optimized using COMSOL Multiphysics software package (COMSOL, Inc.). The actuators consist in rectangular beams made of PDMS elastomer joined to a polymeric substrate (SU-8 epoxy resin) of width  $w$ , length  $l$ , and thicknesses  $h_{AL}$  and  $h_S$  for active layer (PDMS) and substrate (SU-8) respectively.  $S$  denotes the swelling ratio while the Young's modulus, density and Poisson's ratio are defined as  $E$ ,  $\rho$ , and  $\nu$ , respectively. Due to the nonlinear behavior of soft material, kinematic models for traditional rigid bodies are generally not suitable for soft ones. For small deformations, however, linear stress-strain relationships are enough to model the mechanical deformations of soft actuators. For large deformation and especially in the case of complex geometries and their corresponding 3D movements such as curving or twisting resulting from flexional and torsional deformation, nonlinear solid mechanic model using hyperelasticity laws should be implemented.<sup>[36]</sup> Herein, soft actuators that undergo large deformation even at relatively low applied strain value (around 5%) are studied using a simple yet efficient Neo-Hookean model. Successful results are obtained by taking into account the following conditions: (i) an adequate mesh size has to be accurately set. Very fine mesh is inappropriate to model soft actuator structures where thicknesses in the range of tens of micrometers are too thin in comparison to their width (2 mm) and length (20 mm) for convergence. On the contrary, coarse mesh leads to unrealistic displacements. Concretely, a specific mesh works for a precise combination of parameters.

The challenge to model correctly nonlinear large deformations is to define the most appropriate mesh type for each individual parameter variations. (ii) The "shell" layer method reduces the total calculation iterations by constructing directly thin layer without meshing and thus improves the convergence. (iii) The swelling ratio input should be incremented gradually to achieve convergence, especially for 3D movements. In our case, the swelling ratio was increased from 1 to 100% by step of 1% to reach final convergence. For all the following numerical modeling results presented, the swelling ratio is set at 5%.

Firstly, bilayer structures were modeled to investigate the influence of thicknesses and Young's Moduli of the material layers on their movements.  $h_{AL}$  and  $h_S$  were tuned from 10 to 200  $\mu\text{m}$  and their respective Young's modulus varied from 100 kPa to 10 GPa.  $\rho$  was set at 1.30  $\text{g cm}^{-3}$  and  $\nu$  at 0.4. For each thicknesses studied, the largest deformation was reached for a ratio of Young's moduli of the sensitive layer and the substrate following  $E_s = a \cdot E_{AL} + b$  with  $a$  and  $b$  two constants (see Figure S1, Supporting Information). A bilayer structure of 2 mm large and 20 mm long that consists in 10  $\mu\text{m}$  thick substrate of few GPa of Young's Modulus together with an active (sensitive) layer of Young's Modulus around hundreds of kPa was simulated. According to these FEM results, the couple of materials PDMS/SU-8 was selected to offer large deformation in response to various analyte molecules exposure. PDMS has a relatively low Young's Modulus (typically 700 kPa) that can largely be adjusted according to cross-linking level. Its stability toward humidity and temperature, in addition to its ability to swell in response to organic molecules exposure represent remarkable features exceeding numerous hydrogel ones for the development of soft actuators. Subsequently, SU-8 was chosen as substrate material due to its appropriate Young's Modulus value (4 GPa), high chemical inert and its ability to be micro-structured. For that matter, SU-8 rigid stripes of 1 mm large oriented at 30°, 45°, and 60° angle and separated from each other by 1 mm were added on either one or two sides of PDMS layers. Their resulting displacements compared to bilayer actuators are shown in **Figure 1**.

Patterned rigid stripes on a single side of PDMS induce curved displacement due to the contribution of both flexion and torsion forces (Figure 1b). The curving direction depends on the angle of the rigid stripes. Interestingly, double side patterned soft actuators with the top pattern being inversely symmetrical to the down side turns curving into twisting actuation (Figure 1c). Such architecture balances forces and bending moment in the  $z$ -direction applied to the soft actuator so that its out-of-plane ( $z$ -direction) flexional deformation is negligible. It is noteworthy that the elastic strain and stress properties and magnitude of displacement of both one and two side-patterned actuators follow the exact same trend observed for bilayer structures. The design guideline provided by these FEM results that can predict strain distribution in the structure and the resulting deformations was implemented for the fabrication of solvent responsive biomimetic soft actuators.

## 3. Soft Actuator Microfabrication

The fabrication process is relatively simple, making it possible to prepare easily these biomimetic soft actuators (**Figure 2**) with precisely controlled deformations. It consists mainly in

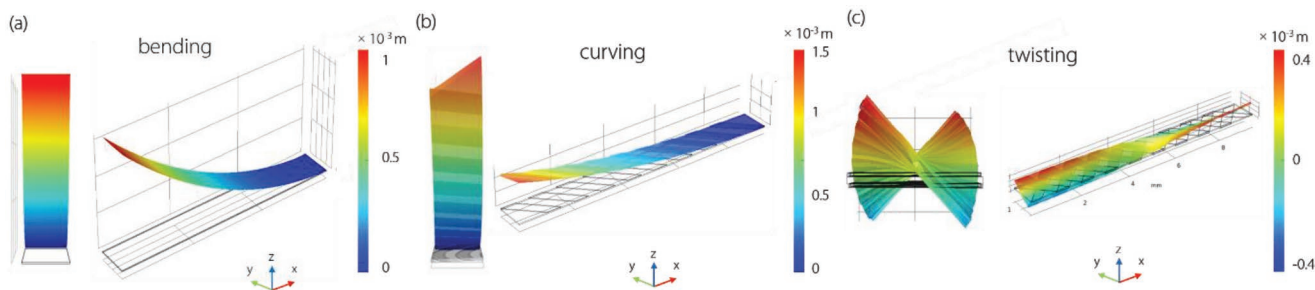


**Figure 1.** FEM results of displacement soft actuators that consist in a) a bilayer structure that induces bending displacement, b) a bilayer structure with one side micropatterned with rigid stripes of 45° angle leading to curving deformation and c) a multilayer structure comprising a PDMS layer sandwiched between two SU-8 layers microstructured in rigid stripes of 45° angle resulting in a twisting movement.

UV-photolithography to pattern SU-8 orientated stripes on one or two sides of a spin-coated PDMS thin film. Further details on the fabrication process are given in the Experimental Section. The key concept of these biomimetic soft actuators relies on the fact that PDMS swells upon molecules absorption when exposed to VOCs while SU-8 is inert, that in turn induces mechanical deformation. Once exposed back to air, the

actuators returned to their initial position due to quick desorption of the uptake molecules. Resulting 3D movements were analyzed from optical images and videos recorded using two Raspberry Pi cameras positioned at 90° angle from each other to capture  $x$  and  $y$  coordinates of the tip end of the soft actuators (Figure 3a,b) placed into glassy transparent chamber for analyte molecules exposure.  $x$  and  $y$  coordinates were treated

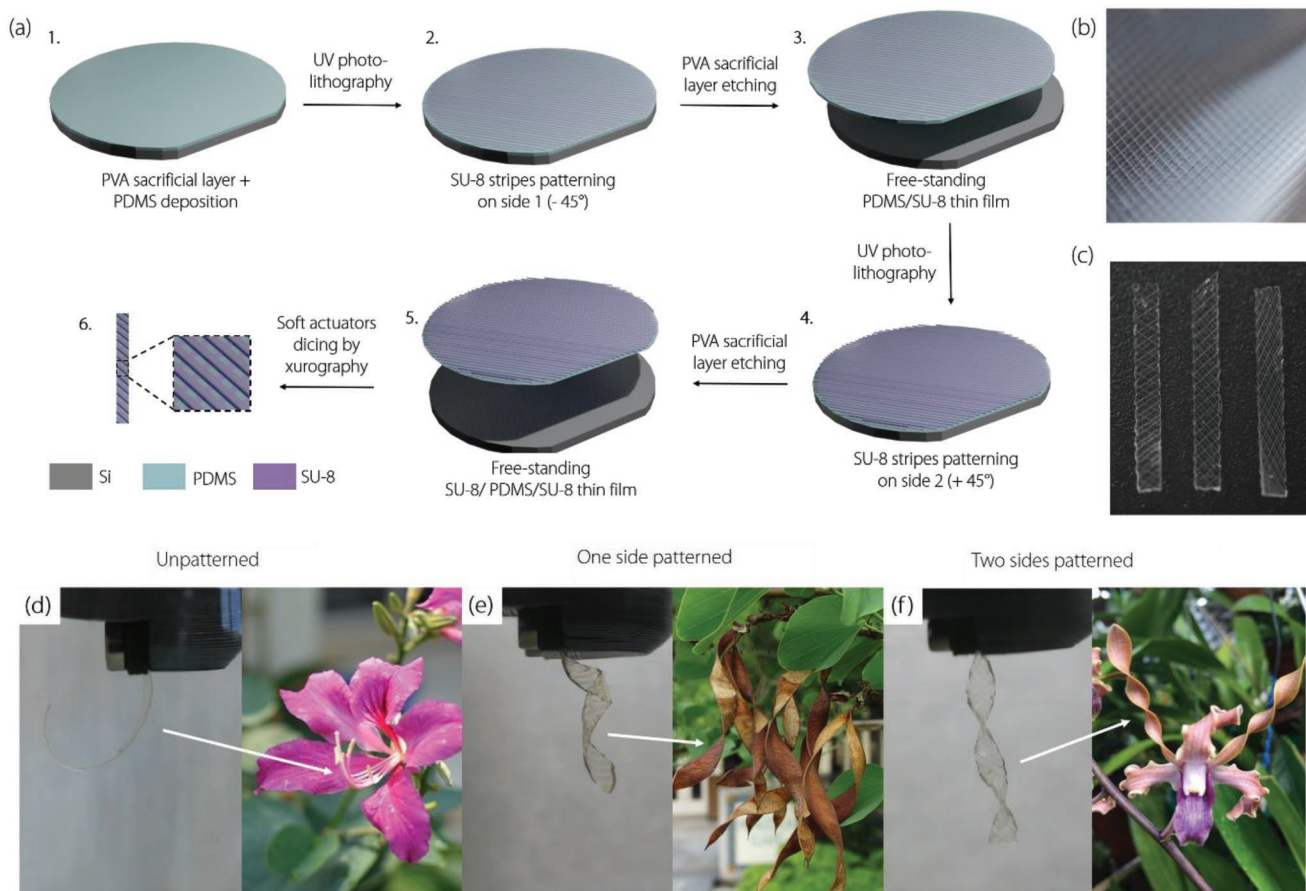


**Figure 2.** Fabrication process of soft actuators a) schematic of the fabrication process flow of soft actuators; b) optical image of the surface of the double side microstructured SU-8 lines onto a free standing PDMS films; c) optical image of three actuators with 30°, 45°, and 60° oriented stripes patterned on both sides; d) Optical image of unpatterned bilayer biomimetic soft actuator exposed to  $n$ -pentane vapors showing bending motion as stamen of *Bauhinia variegata* flowers. e) Optical image of single side patterned biomimetic soft actuator exposed to  $n$ -pentane vapors showing curving motion like *Bauhinia variegata* seed pods in dried state. f) Optical image of double side patterned biomimetic soft actuator exposed to  $n$ -pentane vapors showing twisting motion similarly to *Dendrobium orchids* petal. d,e) Courtesy from selectree.calpoly.edu.

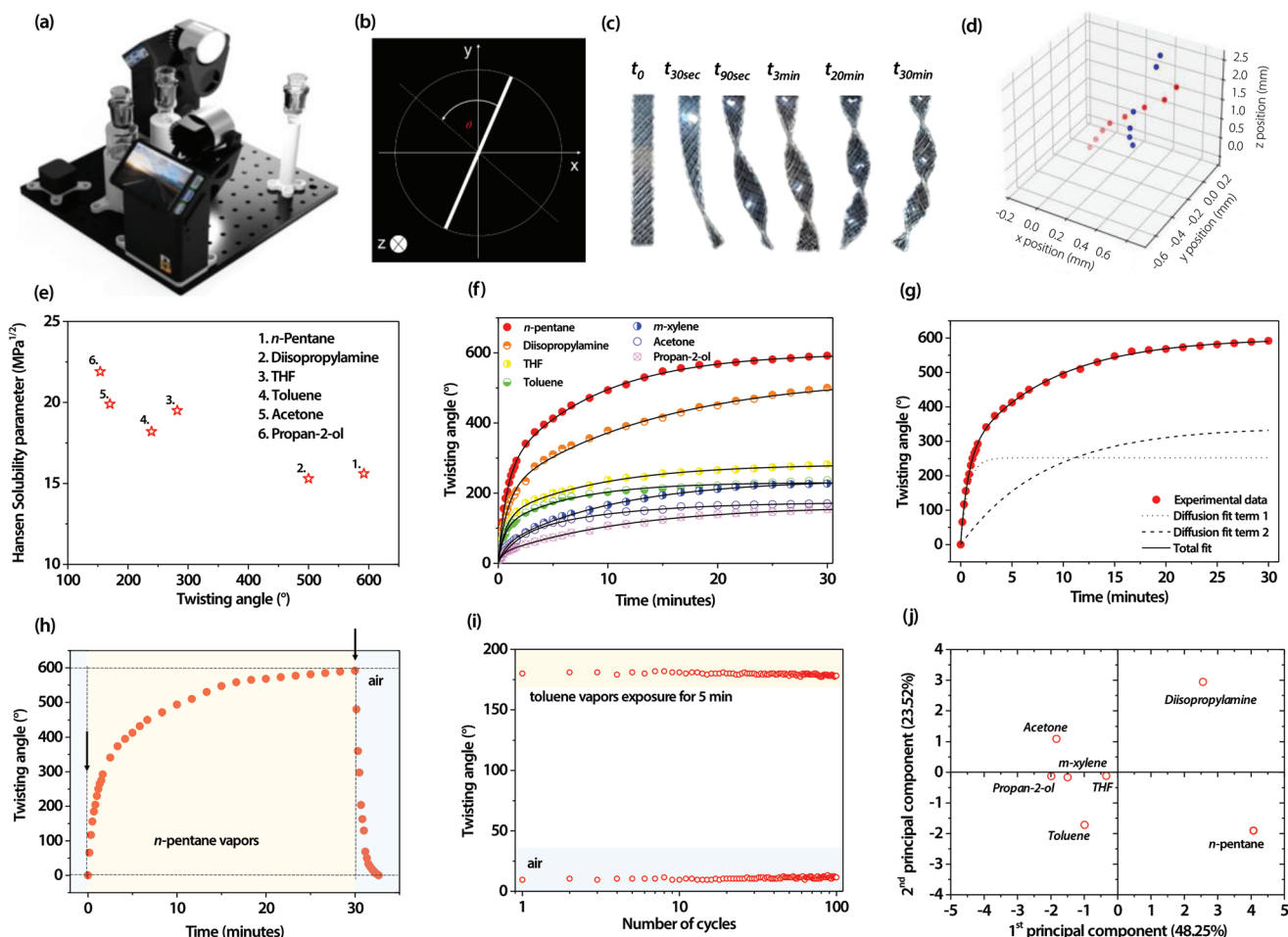


**Figure 3.** Solvent responsive biomimetic soft actuation. a) Optical bench set up to acquire images and videos of 3D actuation. It consists in two Raspberry Pi high quality cameras with 16 mm objectives monitored by two Raspberry Pi 4 microcontrollers positioned at 90° angle for each other to capture x and y motion via an Open-CV Python program able to plot the soft actuator profile 3D actuation, b) three-dimensional space Cartesian coordinate system that depicts how twisting angle were measured, c) optical image of a soft double side patterned soft actuator exposed to *n*-pentane vapors showing twisting motion as a function of time, d) actuator 3D twisting movement measured under *n*-pentane exposure for 100 s, blue and red points representing positions on the right and left edges of the actuator, e) correlation between rotational angle of soft actuators exposed to various vapors of solvents and their respective Hansen solubility parameters, f) experimental kinetic responses and associated analytical fits of the twisting actuation of actuators exposed to different VOCs up to 30 min, g) dual fit response of a soft actuator exposed to saturated vapors of *n*-pentane for 30 min, h) transient response and recovery of a soft actuator exposed to saturated vapors of *n*-pentane and then to air, i) reversibility and reproducibility twisting actuation of an actuator exposed to toluene vapors for 5 min and then to air for 100 cycles, and j) biplot obtained through PCA performed over vapors of solvent sensing kinetic parameter results for seven analyte molecules.

using a home-made Open-CV Python program able to monitor the beam displacement and rotation angle of the actuators (Figure 3c,d, Figure S2 and Video S1, Supporting Information).

Bilayer actuators bent quickly upon increasing analyte molecules exposure time engendering high self-rolling up. For instance, when placed in saturated *n*-pentane vapors for 30 s bilayer actuators showed curvature higher than 1 cm<sup>-1</sup> as shown in Figure 2d. To further achieve complex programmable 3D actuation with enhanced stability, we designed biomimetic smart structures where one or two sides were patterned with rigid lines resulting in curving and twisting displacements inspired by *Bauhinia variegata* seedpods and *Dendrobium orchid* petals respectively (Figure 2e,f). In fact, the curvature motion can be predicted by the angles of the stripes, accordingly to FEM results. As an example, actuators with 30° angle orientated rigid

SU-8 stripes exposed to diisopropylamine vapors for 30 min result in three spins where each coiling are separated with an angle of 30°. Increasing stripes angles from 30° to 60° reduces the numbers of spins from three to one in a 2 cm long actuator (see Figure S3, Supporting Information). In agreement with FEM results, patterning SU-8 in thin stripes reduces the overall strain level experienced by the actuator structure hence, prevents its damaging even for long time exposure (over 30 min). More specifically, double side patterned actuators with asymmetric SU-8 lines on each side demonstrated to enhance further controlled stable and reproducible 3D motion. Doing so cancels out the flexional forces experienced by the actuator and thus suppresses the out-of-plane displacement. Therefore, the actuators experience only torsional forces when exposed to analyte molecules resulting in twisting displacement.

#### 4. From Sorption Based Actuation to Solvent Vapors Sensing

Figure 3a shows the optical bench used to assess the kinetics of actuation of our biomimetic soft actuators of 20 mm long and 2 mm wide. The twisting angles were recorded by tracking the  $x$  and  $y$  coordinates of the tip end of a double side patterned actuator with 45° angle stripes (Figure 3b–d) exposed to seven different solvents at saturation, namely diisopropylamine,  $n$ -pentane, tetrahydrofuran (THF),  $m$ -xylene, toluene, acetone, and propan-2-ol for 30 min as shown in Figure 3f. An exposure time of 30 min was chosen as the rotational angle reached a quasi-steady value for all the solvents vapors tested confirming achieved equilibrium state. The results showed large rotational angles (>500°) were obtained with  $n$ -pentane and diisopropylamine, while moderate angles were achieved for THF,  $m$ -xylene, toluene, acetone, and propan-2-ol with angle varying from 280° to 155°. The excellent reproducibility of these solvent responsive driven actuation is highlighted in Figure S4 (Supporting Information) that depicts the average measured twisting angle and standard deviation for different actuators of the same geometry ( $n = 7$ ). All experiments were carried out at room temperature (20 °C) and 1 atm in a glass chamber of 20 cm<sup>3</sup>. In addition, the soft actuators were shown to be insensitive to temperature below 100 °C and relative humidity in the range 20 to 80 RH%.

The sorption of an analyte molecule within a film depends on the types (gas–film or gas–gas) of interactions and their intensities. The affinity of these interactions determine the quantity of absorbed analyte molecules within a film and associated kinetics. Because SU-8 has negligible interactions with all the solvents tested, only gas–PDMS interactions are analyzed and discussed thereafter. The gas–film partition coefficient  $K$  at equilibrium can be defined by the ratio of the activity of an analyte molecule in a gas phase to its activity in the condensed phase within a film such as:

$$K = \frac{a_{\text{gas/gas}}}{a_{\text{gas/film}}} \quad (1)$$

where  $a_{\text{gas/gas}}$  is the activity of the analyte molecule in gas phase and  $a_{\text{gas/film}}$  the activity of analyte molecule condensed in the film. These activities depend on the polarity, hydrogen bond interactions, dispersion and cavity effects. Obviously, activities have in turn a direct influence on the solubility parameters as well as the diffusion coefficient of an analyte molecule within a

given material. Previous studies have reported the correlation between the solubility parameter and the swelling of PDMS exposed to VOCs in liquid and vapor phases. Whitesides et al. showed that the swelling of PDMS immersed in solvents can be related to the Hildebrand solubility parameters which depend on the cohesive energy of molecules,<sup>[37]</sup> VOCs with a solubility parameter close to that of PDMS inducing the largest swelling. Nevertheless, VOCs with similar solubility parameters do not always result in the same degree of swelling of PDMS due to discrepancy in their polarity. PDMS is hydrophobic and does not swell significantly upon exposure to common polar solvents.<sup>[37]</sup> On the other hand, it has a strong affinity to many non-polar solvents.<sup>[38]</sup> Despite Hildebrand solubility parameters are good guides to measure the compatibility of PDMS with non-polar and slightly polar solvents, they depict incompatibility for polar solvents. Hansen proposed the Hansen solubility parameters ( $\delta$ ) that take into account the dispersion interactions ( $\delta_d$ ), dipolar interactions ( $\delta_p$ ), and hydrogen bonding interactions ( $\delta_h$ ) to correlate more accurately the degree of swelling of PDMS.<sup>[39]</sup> Accordingly, we investigated the evolution of the rotational angle of our actuators versus the Hansen solubility parameters of various vapors of solvents (Figure 3e). Despite the swelling of PDMS exposed to organic vapors has been reported to be linearly correlated with the Hansen solubility parameters,<sup>[40]</sup> herein, we observed a certain discrepancy in the expected linear response of the twisting angle of various soft actuator exposed to saturated vapors of solvents and their corresponding Hansen solubility parameters. This observation may imply that other parameters such as partial pressure of vapors of solvent influence the kinetic response of our actuators.

As expected, we observed that the twisting angle of our soft actuators is higher as the Hansen solubility parameters ( $\delta$ ) get closer to the one of PDMS ( $\delta_i = 16.6$ ). However, this relation between rotational angle and solubility parameters can deviate in some cases as previously reported.<sup>[37]</sup> For instance,  $n$ -pentane and diisopropylamine have similar  $\delta_i$  (15.6 and 15.3 respectively), but one can observe that  $n$ -pentane exhibits significantly larger twisting than diisopropylamine (599° vs 533°). We attributed this discrepancy to the very high partial pressure (57.9 kPa) of  $n$ -pentane in comparison to diisopropylamine (9.3 kPa). In the case of THF and acetone, two solvents with nearly identical  $\delta_i$  and partial pressure (see Table 1), soft actuators exposed to THF vapors twist by an angle of 280° whereas a rotational angle of 170° was measured under acetone exposure. This difference can be explained by the mismatch of polarity of the solvents, namely 0.207 and 0.355 respectively. It

**Table 1.** Characteristic kinetic parameter values for tested vapors of solvents.

Solvent	Twisting angle [°]	$\tau_{\text{res1}}$ [s]	$A_1$	$\tau_{\text{res2}}$ [s]	$A_2$	$\tau_{\text{rec1}}$ [s]	$B_1$	$\tau_{\text{rec2}}$ [s]	$B_2$
$n$ -Pentane	599	44.3	251	459.9	341	39.4	615	N/A	N/A
Diisopropylamine	533	51.9	192	837.9	326	29.4	212	156.4	267
THF	283	41.8	124	535.9	150	59	67	330	67
$m$ -Xylene	227	43.9	45	622.0	190	570	113	685	113
Toluene	230	34.4	101	387.6	125	51	170	748	62
Acetone	175	103.8	69	551.0	99	21	114	42	56
Propan-2-ol	164	23.0	27	709.9	136	N/A	N/A	N/A	N/A

is noteworthy that the total solubility parameter  $\delta_t$  defined by Hansen is the sum of the dispersion interactions ( $\delta_d$ ), dipolar interactions ( $\delta_p$ ), and hydrogen bonding interactions ( $\delta_h$ ) within the material. Although two solvents can have similar  $\delta_t$ , the proportions of  $\delta_d$ ,  $\delta_p$ , and  $\delta_h$  that add up to an identical value of  $\delta_t$  can vary and lead to different swelling ratio. Finally, the molecular size of the analyte molecule can also induce differences in swelling as larger molecules will take longer time to reach equilibrium. Our results suggest that we can classify the impact of the following parameters and the swelling of PDMS and thus the rotational angle of our actuator as such: solubility parameters > polarity > partial pressure.

In order to get further insight into the kinetics of actuation driven by the swelling of PDMS, analytical fits based on a two-rate diffusion process was used to describe the twisting kinetics of the actuator when placed in VOCs saturated vapors as shown in Figure 3g. It represents the overall mass uptake of molecules through the PDMS film that combines the absorption in the film and the diffusion through it as defined by Equation (2). Similarly, Equation (3) can be employed to analytically describe the desorption process.

$$\theta_{\text{up}} = A_1 \left( 1 - e^{-\frac{t}{\tau_{\text{res1}}}} \right) + A_2 \left( 1 - e^{-\frac{t}{\tau_{\text{res2}}}} \right) \quad (2)$$

$$\theta_{\text{down}} = B_1 e^{-\frac{t}{\tau_{\text{rec1}}}} + B_2 e^{-\frac{t}{\tau_{\text{rec2}}}} \quad (3)$$

Each term depends on the solubility parameters, polarizability, its partition coefficient with PDMS, the partial pressure and the geometry of the actuator. When PDMS is exposed to VOCs, analyte molecules are adsorbed at the surface before absorption within the material. Depending on their affinity, molecules can be trapped in specific adsorption sites, while others diffuse freely into the structure. The transport behavior of a given analyte molecule varies from one polymer to another. Transport properties depend on the free volume within the polymer and the segmental mobility of the polymer chains.<sup>[41]</sup> Concretely, Figure 3h shows the transient response/recovery curve of the actuator exposed to saturated vapors of *n*-pentane. Similarly, each experimental actuation motion transient curve obtained from the actuator for tested vapors of solvents are presented in Figure S5 (Supporting Information). In our case, the swelling kinetics of PDMS is characterized by a steep slope as a function of time up to a first level of saturation (Figure 3g). The first diffusion coefficient term,  $\tau_{\text{res1}}$ , describes both adsorption and absorption resulting in a significant swelling of the film. We assume that the diffusion of analyte molecules within the film gets faster in a swollen state. The first absorbed molecules pave the way for the following ones, which penetrate within the film faster. Consequently, another kinetics,  $\tau_{\text{res2}}$ , occurs at a slower rate, which is about one order of magnitude larger than  $\tau_{\text{res1}}$  and consists in the rearrangement of polymer chains caused by penetrating diffusion.<sup>[42]</sup> The voids in the PDMS structure are continuously redistributed. The increase in volume by swelling also accelerates this rearrangement, where the two phenomena support each other.

The absorption and desorption curves for the seven analyte molecules tested were fitted with the two-rate diffusion model

given by Equations (2) and (3) to obtain diffusion coefficients  $\tau_{\text{res1}}$  and  $\tau_{\text{res2}}$ , desorption coefficients  $\tau_{\text{rec1}}$  and  $\tau_{\text{rec2}}$  as well as magnitude coefficients  $A_1$ ,  $A_2$  and  $B_1$ ,  $B_2$  given in Table 1. The obtained fit based on these kinetics parameters reflecting the actuation dynamics, agree well with our experimental data. Figure 3h and Table 1 show that the absorption and desorption kinetics differ. The kinetics of adsorption and desorption can be defined by an equilibrium relationship where constant kinetics of absorption ( $K_a$ ) and desorption ( $K_d$ ) take part. While  $K_a$  depends on the temperature and the partial vapor pressure,  $K_d$  depends only on the temperature. This can explain the difference observed in time constant between absorption and desorption. For desorption, absorbed analyte molecules redistribution in the bulk is negligible. Shrinking of PDMS during desorption accelerates the rearrangement of the polymer chains. Figure 3i shows that reproducible programmable actuation was successfully asset by recording a reversible and repeatable twisting angle of  $177^\circ \pm 3^\circ$  exposed to saturated toluene vapors for 5 min after 100 cycles.

Reciprocally, twisting movements of these soft actuators allow to sense and partially discriminate a variety of vapors of solvents from their environment. As explained previously, the interaction of an analyte molecule with the sensing material depends on solubility parameters, polarity and partition coefficient, which in turn results in distinct transient response and recovery characteristics. The kinetics parameters (twisting angle ( $\theta$ ), tip end velocity ( $V_t$ ),  $\tau_{\text{res1}}$ ,  $\tau_{\text{res2}}$ ,  $A_1$ ,  $A_2$ ,  $\tau_{\text{rec1}}$ ,  $\tau_{\text{rec2}}$ ,  $B_1$ , and  $B_2$ ) listed in Table 1 were employed to generate a  $7 \times 9$  matrix (7 analyte molecules and 9 parameters). This set of data was used as inputs in principal component analysis (PCA) to get a biplot allowing to discriminate analyte molecules (see Figure S6, Supporting Information).<sup>[43,44]</sup> Figure 3j shows that four analyte molecules scatter distinguishably in PCA space. Precisely, Diisopropylamine, Acetone, Toluene, and *n*-pentane are placed in the first, second, third, and fourth quadrant respectively which facilitates their discrimination. THF is located close to the center while *m*-xylene and Propan-2-ol are grouped near the overlapping region I and II rendering their identification more complicated.

## 5. Origami Biomimetic Soft Actuators

To expand the potential of solvent responsive actuators, untethered double side patterned soft structures of complex shapes such as cross, triangle, circle, and star (Figure 4a–d) that bend under solvent vapors absorption were fabricated. Interestingly, we observed that their actuation when exposed to *n*-pentane for a minute, points toward the direction of the tip of longer axe of the structure and then decreases. Concretely, we can assure that by simply choosing the appropriate shape of a structure, it is possible to control its direction of motion.

In order to broaden the accessible 3D shapes of solvent responsive soft actuators, we also considered an origami approach by adding creases that behave as hinges in the structures and providing further flexibility and novel controlled motion in specific directions. Figure 4e shows a snake like soft continuum actuator which design makes tangential curves (*S* shape) along its length when exposed to VOCs.

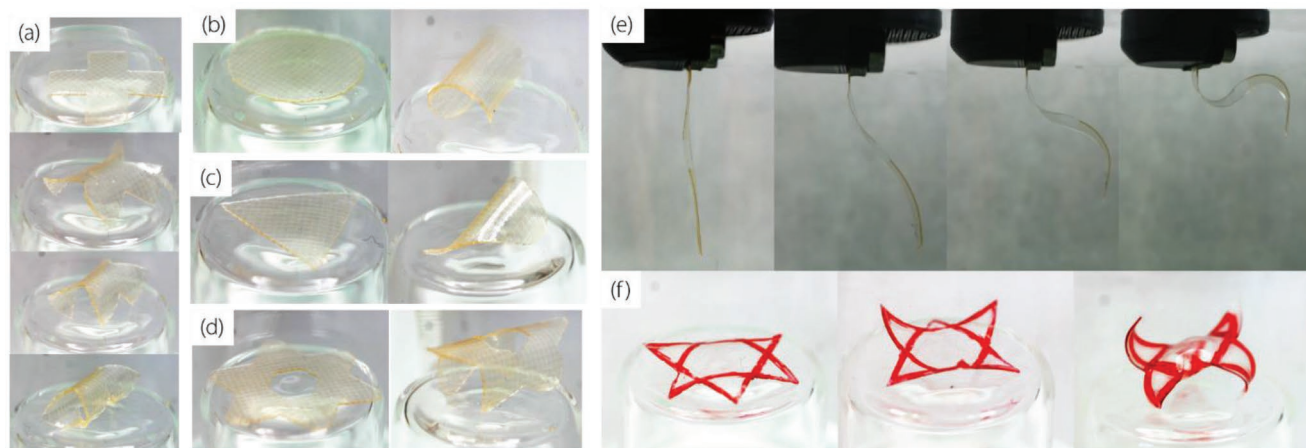


**Figure 4.** Origami based soft actuators. Optical images of double sides patterned soft structures of various shapes such as a) cross, b) circle, c) triangle, d) star at initial state and after a minute exposure to *n*-pentane vapors, e) optical images of the evolution of corrugated deformation of a “snake” like soft actuator exposure to *n*-pentane vapors for 60 s, and f) optical images of dual walker–grripper soft actuator exposure to *n*-pentane vapors for 60 s.

Herein, the origami used consisted in patterning half of the actuator length with an SU-8 inert layer on one side coupled with another SU-8 layer of identical thickness on the other side of the second half of the actuator. This origami pattern adds redundancy that increases the number of degrees of freedom, enabling corrugated deformation along the actuator length and thus continuous change in bending profiles, which offers specific functionality for soft actuators. In contrast to pneumatic actuators where all sections are actuated from the base, our solvent responsive biomimetic soft actuators exhibit degrees of freedom that are only dependent on the pattern which are not limited to the size of the actuator. Additionally, a dual walker–grripper soft actuator was fabricated as shown in Figure 4f. The pattern of this star shaped actuator consists in a PDMS film sandwiched between two hollow triangles whose extremities contain a thin SU-8 line that acts as hinges. When exposed to solvent vapors the tips of each triangle bend toward opposite directions and play the role of legs or arms allowing a dual walker–grripper functions. Such soft devices find promising applications as manipulator or gripper able to catch and release an object as well as walkers showing displacement ability under repeated VOC exposure cycles. There are strong requirements for alternative options to electrical or magnetic field as well as pneumatics and hydraulics driven actuation of complex and rigid components while miniaturizing the actuators.

## 6. Conclusion

This work demonstrated molecularly driven biomimetic soft continuum actuators able to bend, curve and twist when exposed to solvent vapors. Such highly reversible and addressable 3D mechanical deformations were predicted by defining accurately mechanical asymmetries in the actuators. A novel route for designing smart actuators with a precise and complex movement was assessed by finite element modeling and their resulting motion was validated experimentally. In particular, we investigated the influence of the geometry and

orientation of micropatterned strips of resins-8 employed as structural layer onto a PDMS sensitive layer that swells under molecule absorption. Reciprocally, these soft actuators can simultaneously sense a variety of analyte molecules from their environment and discriminate them by analyzing their movements with PCA. Finally, additional 3D motions were achieved using an origami approach by adding creases that behave as hinges in soft structures providing further flexibility and novel controlled motion in specific directions in continuum structures.

## 7. Experimental Section

**Materials:** PDMS (Sylgard184) and crosslinkers were purchased from Neyco. Epoxy-based photoresists (SU-8 2002, 3010, and 3050) and their developer were purchased from Kayaku Advanced Materials Incorporation. All the organic solvents, including diisopropylamine, *n*-pentane, toluene, Tetrahydrofuran (THF), acetone, isopropanol, and methanol were purchased from Sigma-Aldrich.

**Soft Actuator Fabrication:** Silicon (Si) wafer coated with a thin layer of polyvinyl alcohol (PVA) used as sacrificial layer was employed as sample holder. Then, polydimethylsiloxane (PDMS) was deposited by spin coating, cured in an oven (80 °C, 60 min) under vacuum to obtain a 10 μm thick film. After, SU-8 epoxy-based photoresist (SU-8 3010 purchased from Kayaku Advanced Materials, Inc.) was spin-coated (2000 rpm, 60 s) on top of the PDMS layer previously treated by UV Ozone for 10 min to enhance film adhesion, yielding to a 10 μm thick film. The wafer was soft-baked (95 °C, 3 min) before exposure and subsequently cross-linked by UV photolithography (100 mJ cm<sup>-2</sup>). Then, the film was post-exposure-baked (65 °C, 1 min and 95 °C, 3 min), developed (3 min), and finally rinsed with 1-propanol and DI water. The hybrid film was peeled off by removal of the PVA sacrificial layer in a water bath (10 min) and air-dried. The obtained free-standing bilayer film was flipped over and placed onto a Si-PVA wafer holder. An additional layer of SU-8 was deposited onto the other side of the PDMS layer and subsequently patterned by UV photolithography in the exact same aforementioned conditions.

**3D Actuation Characterization:** Optical images and videos were recorded using two Raspberry Pi high quality cameras with 16 mm objectives monitored by two Raspberry Pi 4 microcontrollers positioned at 90° to capture *x* and *y* motion via an Open-CV Python program able to reproduce in 3D the actuation. Movements were detected by color image processing of the tip end (or the overall edges) of soft actuators.

Images were recorded every 10 s. The relative's coordinate's errors were as low as 2 pixels without affecting angle measurements. Also, a self-correction program was implemented to improve recordings.

**Statistical Analysis:** All data were extracted and analyzed with excel. Mean and standard deviation were taken among 7 samples ( $n=7$ ). The statistical analysis was performed using Principal Component Analysis with the software XLSTAT.

## Supporting Information

Supporting Information is available from the Wiley Online Library or from the author.

## Acknowledgements

The research leading to these results was financed by ANR DEFORM (ANR-18-CE24-0020-01). The authors acknowledge the Equipex ELORPrintTec ANR-10-EQPX-28-01 for the microfabrication of the soft actuators. They also gratefully acknowledge Dr. Marco Pereira (Binary Design3d) for his help in the optical bench set up conception.

## Conflict of Interest

The authors declare no conflict of interest.

## Data Availability Statement

The data that support the findings of this study are available on request from the corresponding author. The data are not publicly available due to privacy or ethical restrictions.

## Keywords

biomimetic sensor, Soft actuator, volatile organic compounds

Received: June 20, 2022

Revised: August 8, 2022

Published online: September 16, 2022

- [1] D. Trivedi, C. D. Rahn, W. M. Kierb, I. D. Walker, *Appl. Bionics Biomech.* **2008**, *5*, 99.
- [2] S. A. Gladman, E. A. Matsumoto, R. G. Nuzzo, L. Mahadevan, J. A. Lewis, *Nat. Mater.* **2016**, *15*, 413.
- [3] X. Huang, K. Kumar, M. K. Jawed, A. M. Nasab, Z. Ye, W. Shan, C. Majidi, *Sci. Rob.* **2018**, *3*, 7557.
- [4] S. Poppinga, C. Zollfrank, O. Prucker, J. Rühle, A. Menges, T. Cheng, T. Speck, *Adv. Mater.* **2017**, *30*, 1870135.
- [5] M. Schaffner, J. A. Faber, L. Pianegonda, P. A. Rühls, F. Coulter, A. R. Studart, *Nat. Commun.* **2018**, *9*, 878.
- [6] Y. Cheng, K. Ren, D. Yang, J. Wei, *Sens. Actuators, B* **2018**, *225*, 3117.
- [7] Y. Zhang, J. Liao, T. Wang, W. Sun, Z. Tong, *Adv. Funct. Mater.* **2018**, *28*, 1707245.
- [8] C. Yao, Z. Liu, C. Yang, W. Wang, X. J. Ju, R. Xie, L. Y. Chu, *Adv. Funct. Mater.* **2015**, *25*, 2980.
- [9] H. Cheng, F. Zhao, J. Xue, G. Shi, L. Jiang, L. Qu, *ACS Nano* **2016**, *10*, 9529.
- [10] S. Janbaz, R. Hedayati, A. A. Zadpoor, *Mater. Horiz.* **2016**, *3*, 536.
- [11] Z. Ji, C. Yan, B. Yu, X. Zhang, M. Cai, X. Jia, X. Wang, F. Zhou, *Adv. Mater. Technol.* **2019**, *4*, 1800713.
- [12] D.-D. Han, Y.-Q. Liu, J.-N. Ma, J.-W. Mao, Z.-D. Chen, Y.-L. Zhang, H.-B. Sun, *Adv. Mater. Technol.* **2018**, *3*, 1800258.
- [13] Y. Dong, J. Wang, X. Guo, S. Yang, M. O. Ozen, P. Chen, X. Liu, W. Du, F. Xiao, U. Demirci, B.-F. Liu, *Nat. Commun.* **2019**, *10*, 4087.
- [14] Z. Lei, W. Zhu, S. Sun, P. Wu, *Nanoscale* **2016**, *8*, 18800.
- [15] D.-D. Han, Y.-L. Zhang, Y. Liu, Y.-Q. Liu, H.-B. Jiang, B. Han, X.-Y. Fu, H. Ding, H.-L. Xu, H.-B. Sun, *Adv. Funct. Mater.* **2015**, *25*, 4548.
- [16] S. J. Aßhoff, F. Lancia, S. Iamsaard, B. Matt, T. Kudernac, S. P. Fletcher, N. Katsonis, *Angew. Chem.* **2017**, *56*, 3261.
- [17] R. Lan, J. Sun, C. Shen, R. Huang, Z. Zhang, C. Ma, J. Bao, L. Zhang, L. Wang, D. Yang, H. Yang, *Adv. Funct. Mater.* **2020**, *30*, 2000252.
- [18] C. Ma, W. Lu, X. Yang, J. He, X. Le, L. Wang, J. Zhang, M. J. Serpe, Y. Huang, T. Chen, *Adv. Funct. Mater.* **2018**, *28*, 1704568.
- [19] Q. Zhao, J. W. C. Dunlop, X. Qiu, F. Huang, Z. Zhang, J. Heyda, J. Dzubiella, M. Antonietti, J. Yuan, *Nat. Commun.* **2014**, *5*, 4293.
- [20] T. Wu, J. Li, J. Li, S. Ye, J. Wei, J. Guo, *J. Mater. Chem. C* **2016**, *4*, 9687.
- [21] L. Zhang, P. Naumov, X. Du, Z. Hu, J. Wang, *Adv. Mater.* **2017**, *29*, 1702231.
- [22] L. Montero de Espinosa, W. Meesorn, D. Moatsou, C. Weder, *Chem. Rev.* **2017**, *117*, 12851.
- [23] A. Miriyev, K. Stack, H. Lipson, *Nat. Commun.* **2017**, *8*, 596.
- [24] S. Coyle, C. Majidi, P. LeDuc, K. J. Hsia, *Extreme Mech. Lett.* **2018**, *22*, 51.
- [25] C. D. Jones, J. W. Steed, *Chem. Soc. Rev.* **2016**, *45*, 6546.
- [26] Y. Yang, Y. Wu, C. Li, X. Yang, W. Chen, *Adv. Intell. Syst.* **2020**, *2*, 2000025.
- [27] X. Le, W. Lu, J. Zhang, T. Chen, *Adv. Sci.* **2019**, *6*, 1801584.
- [28] S. Seethapathy, T. Górecki, *Anal. Chim. Acta* **2012**, *750*, 48.
- [29] A. Kloskowski, M. Pilarczyk, J. Namieśnik, *Anal. Chem.* **2009**, *81*, 7363.
- [30] Q. Huang, T. Deng, W. Xu, C. K. Yoon, Z. Qin, Y. Lin, T. Li, Y. Yang, M. Shen, S. M. Thon, J. B. Khurgin, D. H. Gracias, *Adv. Intell. Syst.* **2020**, <https://doi.org/10.1002/aisy.202000195>.
- [31] R. Fernandes, D. H. Gracias, *Adv. Drug Delivery Rev.* **2012**, *64*, 1579.
- [32] A. Azam, K. E. Laflin, M. Jamal, R. Fernandes, D. H. Gracias, *Biomed. Microdevices* **2011**, *13*, 51.
- [33] T. Manen, S. Janbaz, M. Ganjian, A. A. Zadpoor, *Mater. Today* **2020**, *32*, 59.
- [34] O. Erol, A. Pantula, W. Liu, D. H. Gracias, *Adv. Mater. Technol.* **2019**, *4*, 1900043.
- [35] D. H. Gracias, *Curr. Opin. Chem. Eng.* **2013**, *2*, 112.
- [36] M. S. Xavier, A. J. Fleming, Y. K. Yong, *Adv. Intell. Syst.* **2021**, *3*, 2000187.
- [37] J. N. Lee, C. Park, G. M. Whitesides, *Anal. Chem.* **2003**, *75*, 6544.
- [38] J. Pawliszyn, *J. Chromatogr. Sci.* **2000**, *38*, 270.
- [39] C. M. Hansen, *Hansen Solubility Parameters: A User's Handbook*, CRC press, Boca Raton **2007**.
- [40] C. V. Rumens, M. A. Ziai, K. E. Belsey, J. C. Batchelor, S. J. Holder, *J. Mater. Chem. C* **2015**, *3*, 10091.
- [41] S. C. George, S. Thomas, *Prog. Polym. Sci.* **2001**, *26*, 985.
- [42] J. E. Saunders, H. Chen, C. Brauer, M. Clayton, H.-P. Looock, *Soft Matter* **2018**, *14*, 2206.
- [43] S. Acharyya, S. Nag, S. Kimbahun, A. Ghose, A. Pal, P. K. Guha, *ACS Sens.* **2021**, *6*, 2218.
- [44] A. S. R. Murthy, D. Pathak, G. Sharma, K. I. Gnanasekar, V. Jayaraman, A. M. Umarji, T. Gnanasekaran, *Anal. Chim. Acta* **2015**, *892*, 175.